Editors' Suggestion

Evolution of two-time correlations in dissipative quantum spin systems: Aging and hierarchical dynamics

Stefan Wolff,[1] Jean-Sébastien Bernier,[1] Dario Poletti,[2] Ameneh Sheikhan,[1,*] and Corinna Kollath[1]

[1]*Physikalisches Institut, University of Bonn, Nussallee 14-16, 53115 Bonn, Germany*

[2]*Science and Math Cluster and EPD Pillar, Singapore University of Technology and Design, 8 Somapah Road, 487372 Singapore*

(Received 24 September 2018; published 29 October 2019)

We consider the evolution of two-time correlations in the quantum XXZ spin chain in contact with an environment causing dephasing. Extending numerically exact, time-dependent matrix product state techniques to consider the dynamics of two-time correlations within dissipative systems, we uncover the full quantum behavior for these correlations along all spin directions. Together with insights from adiabatic elimination and kinetic Monte Carlo, we identify three dynamical regimes. For initial times, their evolution is dominated by the system unitary dynamics and depends on the initial state and the Hamiltonian parameters. For weak spin-spin interaction anisotropy, after this initial dynamical regime, two-time correlations enter an algebraic scaling regime signaling the breakdown of time-translation invariance and the emergence of aging. For stronger interaction anisotropy, these correlations first go through a stretched exponential regime before entering the algebraic one. Such complex relaxation arises due to the competition between the proliferation dynamics of energetically costly excitations and their motion. As a result, dissipative heating dynamics of spin systems can be used to probe the entire spectrum of the underlying Hamiltonian.

DOI: 10.1103/PhysRevB.100.165144

I. INTRODUCTION

Two-time correlations are powerful tools to capture the fundamental dynamical features of many-body systems both in and away from equilibrium. These correlation functions are of the form $\langle B(t_2)A(t_1)\rangle$, where A and B are operators, t_1 and t_2 are two different times, and $\langle \dots \rangle = \mathrm{tr}(\rho \dots)$ is the average over the density matrix ρ of a given system. Numerous experimental techniques have been developed to probe these correlations, measuring the response of many-body systems [1–6].

Theoretically, two-time correlations have been studied in isolated many-body quantum systems (i.e., not in contact with an environment), both in and far from equilibrium. These correlations provide information on various spectral features such as collective excitations and bound state and are one of the few observables capturing properties of aging dynamics of classical spin glasses [7]. However, for large open many-body quantum systems (i.e., in contact with an environment), evaluating out-of-equilibrium two-time correlations has proven extremely challenging. Most works have instead focused on characterizing the nonequilibrium dynamics of open systems by considering the universal scaling behavior of simpler observables or the propagation of single-time correlations [8,9] by using various approximate approaches to evaluate two-time correlations [10–16], by focusing on a specific initial time [17], or by considering small many-body quantum systems [18].

Here we evaluate, in a numerically exact manner, the evolution of both the two-time correlations along the z spin direction, $\langle S^z_l(t_2)S^z_{l+d}(t_1)\rangle$, and along the $\pm$ spin directions, $\langle S^+_l(t_2)S^-_{l+d}(t_1)\rangle$, in a quantum XXZ spin-1/2 chain in contact with a memoryless environment causing dephasing. S^z_l and $S^\pm_l$ are the spin-1/2 operators in the z and $\pm$ directions at site l.

The XXZ spin-1/2 chain is a paradigmatic model of theoretical quantum many-body physics. This model is particularly well suited to investigate new phenomena and can be considered as a foundational building block to which various coupling terms can be added. We employ it to gain insights into the interplay of interaction effects and dissipative couplings. While spin chains were at first thought to be mostly relevant in the context of solid-state physics, e.g., in organic materials [19], recent experimental advances have made it possible to engineer these systems using ultracold atomic gases in optical lattices [20–25] and Rydberg states [26]. For example, various aspects of the quantum spin dynamics occurring in XXZ spin-1/2 chains, such as the motion of magnons and spin transport, have been investigated using cold atomic gases in optical lattices (see Ref. [27] and references therein). Furthermore, an environment coupling causing dephasing does arise in cold atomic gases in optical lattices or in Rydberg atoms due to the presence of fluctuating light fields [28–30], and this effect can be enhanced by tailoring the application of such fields.

Previous theoretical works on the XXZ spin-1/2 chain with dephasing had solely focused on the evaluation of equal-time correlations along the $\pm$-spin directions [31], identifying an algebraic regime similar to the one found for interacting bosons in contact with a dissipative environment causing dephasing [32,33]. Additionally, in the classical limit, for large interaction anisotropies, the $\langle S^z_l(t)S^z_l(0)\rangle$ correlations were shown to display a stretched exponential behavior [13].

*Corresponding author: asheikhan@uni-bonn.de

We developed here a variant of the numerically exact time-dependent variational matrix product state (t-MPS) technique [34,35] applicable to two-time correlation in open systems taking conservation laws into account. Using this approach, we uncover the full quantum behavior of these correlations along both the z and the $\pm$ spin directions when the evolution of the spin system begins from an excited state such as the Néel $|\uparrow,\downarrow,\uparrow,\downarrow,\ldots,\uparrow,\downarrow\rangle$ or the single domain wall state $|\uparrow,\ldots,\uparrow,\uparrow,\downarrow,\downarrow,\ldots,\downarrow\rangle$.

We identify three interesting dynamical regimes signaled by changes in the behavior of the two-time correlations along the z spin direction. The first regime, identified at initial times, is dominated by the system unitary dynamics. This regime depends significantly on the initial state and on the Hamiltonian parameters, and, for weak dissipation, resembles the dynamics of the isolated system. The second regime, identified both numerically and analytically, is characterized by an algebraic scaling: for distances $d \geqslant 1$, the normalized correlations are proportional to $(t_2/t_1)^{-3/2}$, signaling the emergence of aging dynamics with broken time-translation invariance. In this particular case, this aging regime finds its origin in the presence of underlying diffusive processes. Finally, in the third regime, correlations evolve following a stretched exponential, a behavior typically associated with glasses or systems exhibiting hierarchical separation of timescales. This regime, which we identify over a wide range of t_1 using numerically exact simulations, occurs only for sufficiently strong interaction anisotropies when the evolution begins from initial states with occupied energy levels well separated from others. The evolution of these two-time correlations is governed by the competition between the nucleation (or annihilation) dynamics of energetically costly excitations and their motion, two processes occurring on very different timescales.

We interpret our numerically exact numerical findings using adiabatic elimination and kinetic Monte Carlo, from which the scaling properties can be predicted, and find the observed dynamics to closely relate to the spectrum of the spin Hamiltonian. Monitoring the dynamics of two-time correlations induced by dissipative heating can thus be used to characterize spin systems as it reveals features spanning the entire spectrum of the underlying Hamiltonian. Let us also mention that the two-time correlations along the $\pm$ spin direction decay exponentially and therefore exhibit a completely different behavior from which the regimes mentioned earlier cannot be inferred.

II. INTERPLAY OF UNITARY AND DISSIPATIVE DYNAMICS

To investigate the nonequilibrium dynamics of two-time correlations in an open quantum system, we consider a spin-1/2 chain under the effect of local dephasing noise. In this system, the evolution of the density operator ρ is described by the Lindblad master equation

$$\frac{\partial \rho}{\partial t} = -\frac{i}{\hbar}[H_{\mathrm{XXZ}}, \rho] + \mathcal{D}(\rho). \tag{1}$$

The first term on the right-hand side describes the unitary evolution due to the XXZ spin-1/2 Hamiltonian,

$$H_{\mathrm{XXZ}} = \sum_{j=1}^{L-1} \left[J_x\left(S_j^x S_{j+1}^x + S_j^y S_{j+1}^y\right) + J_z S_j^z S_{j+1}^z\right],$$

where J_x and J_z are the exchange couplings along the different spin directions, S_j^α is the α-direction spin operator at site j, and L is the length of the chain. Similar setups can be readily realized in state-of-the-art ultracold atom experiments [28–30]. The isolated XXZ spin chain is solvable by Bethe ansatz and is known to present three distinct phases [36]: for $-1 \leqslant J_z/J_x \leqslant 1$, the easy plane anisotropic phase is gapless, while $J_z/J_x < -1$ presents a gapped ferromagnetic phase, and $J_z/J_x > 1$ hosts a gapped antiferromagnetic phase. The second term on the right-hand side of Eq. (1) describes the dephasing noise in Lindblad form,

$$\mathcal{D}(\rho) = \gamma \sum_{j=1}^{L} \left(S_j^z \rho S_j^z - \frac{1}{4}\rho\right),$$

where γ is the dissipation strength. This term induces spin fluctuations and eventually drives the system towards the infinite temperature state, the unique steady state of the model. If not stated otherwise, we consider here a system initially prepared in the Néel state and investigate its dynamics as the system is coupled to the environment and starts to undergo dephasing. We access, in a numerically exact manner, the full quantum dynamics of this dissipative system by extending the currently available t-MPS techniques to the study of two-time correlations taking good quantum numbers into account. Our analysis is carried out using an implementation of t-MPS built upon the ITensor library [37]. The density matrix operator is represented as a pure state in an enlarged Hilbert space, and the evolution of the two-time correlations is implemented, adapting the approach used to obtain their equilibrium thermal counterparts [38,39]. Taking good quantum numbers into account [9,40] enables us to follow the numerically exact evolution for sufficiently long times (see Appendix D for the technical details).

To gain analytical insights into the evolution of this system, we employ adiabatic elimination, valid for times larger than $1/\gamma$, to capture the dominant dissipative dynamics in the limit where $\hbar\gamma \gg J_z$. We focus primarily on the two-time correlations along the z-spin direction given by

$$\hbar^2 C_d(t_2, t_1) = \left\langle S^z_{\frac{L}{2}}(t_2) S^z_{\frac{L}{2}+d}(t_1)\right\rangle,$$

where d is the distance between two spins, as they provide the most insights into the dynamical properties of the system, and we also investigate the corresponding equal-time correlations.

III. EMERGENCE OF THREE DISTINCT DYNAMICAL REGIMES

As hinted earlier, we find the normalized two-time correlations along z-spin direction to present three distinct dynamical regimes depending on the dissipation strength, $\hbar\gamma/J_x$, and the interaction anisotropy, J_z/J_x. For weak dissipation, the initial time regime is governed by the system unitary dynamics. For strongly interacting systems, the dynamics is typically

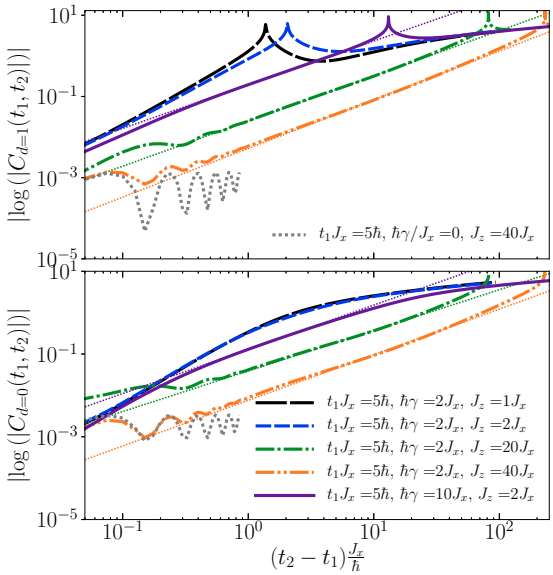

FIG. 1. Initial quasiunitary and intermediate stretched exponential regimes. Logarithm of the two-time correlation $\hbar^2 C_d(t_2,t_1) = \langle S^z_{\frac{L}{2}}(t_2) S^z_{\frac{L}{2}+d}(t_1)\rangle$ for $d=1$ (upper panel) and $d=0$ (lower panel) vs the time difference t_2-t_1 (t-MPS data for $L=48$). For weak dissipation, the initial time regime is dominated by the system unitary dynamics (dashed gray line). The dephasing noise damps out the oscillations commonly present in the unitary evolution. Following this initial regime, for sufficiently strong coupling anisotropy J_z/J_x, the two-time correlations follow a stretched exponential: the linear slopes indicate the presence of this regime. The thin dotted lines are fits in the linear regions. The data has been obtained for a Trotter time step of $\Delta t J_x/\hbar = 0.025$ and a truncation error of $\epsilon = 10^{-12}$.

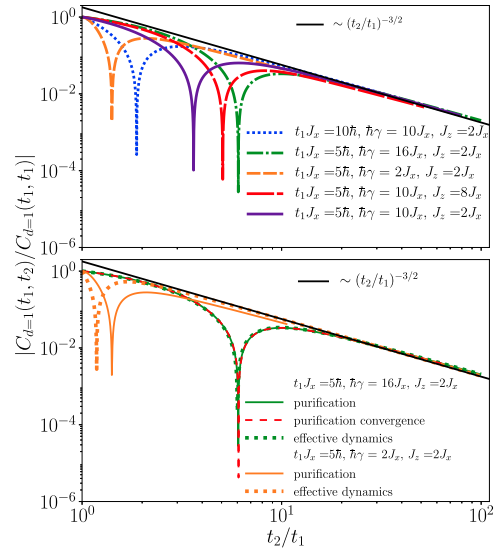

FIG. 2. Scaling regime for the two-time correlations. (Upper panel) Scaling collapse for the normalized two-time correlations between neighboring sites $\hbar^2 C_{d=1}(t_2,t_1) = \langle S^z_{\frac{L}{2}}(t_2) S^z_{\frac{L}{2}+1}(t_1)\rangle$ calculated using t-MPS. The black solid line is a guide to the eye and highlights the $(t_2/t_1)^{-3/2}$ algebraic regime. (Lower panel) Comparison between the two-time correlations obtained from t-MPS and adiabatic elimination. For large $\hbar\gamma/J_z$ ratios, adiabatic elimination describes two-time correlations over the whole range of t_2/t_1, whereas for smaller ratios, the analytical approach successfully captures the long-time $(t_2/t_1)^{-3/2}$ scaling but fails to describe the initial dynamics. The calculations are preformed for a system length $L=80$, a Trotter time step $\Delta t J_x/\hbar = 0.025$, and a truncation error $\epsilon = 10^{-12}$. For comparison, the line "purification convergence" is shown for $L=90$, $\Delta t J_x/\hbar = 0.0125$, $\epsilon = 10^{-13}$.

characterized by oscillations due to the opening of a gap in the energy spectrum. Such dynamics, illustrated by the gray dotted lines in Fig. 1, is damped by the dephasing. The other curves shown in Fig. 1 will be discussed in detail later.

After this initial unitarylike evolution, the system enters a scaling regime where the two-time correlations break time-translation invariance as they do not depend on t_2-t_1. This regime, which occurs at later times for stronger interaction strengths, is exemplified in Fig. 2 where the correlations for $d=1$ are shown. For $d=1$, the normalized two-time correlations scale as $\sim(t_2/t_1)^{-3/2}$, and one can see that there is a regime for which curves with different t_1, γ, and J_z nicely collapse on top of each other. As this region is characterized by the slow algebraic relaxation of correlations and by a dynamical scaling that is solely a ratio of t_2/t_1, this system presents emergent aging dynamics. In this regime, the numerical convergence of the MPS method is very good up to long times such that the algebraic scaling can be accurately extracted (see the comparison curve in the lower panel of Fig. 2 and Appendix D for further details). As for $d=0$, we find in this case that the two-time correlations also scale algebraically; however, they do not depend solely on a t_2/t_1 ratio. As explained in the Appendix, these scaling regimes arise when t_1 lies within an interval where the equal-time correlations along the z-spin direction decay algebraically.

To identify the origin of the scaling regime, we use many-body adiabatic elimination [32,41] to develop a set of differential equations capturing the evolution around the dissipation-free subspace (see Appendixes A–C for more details). Then, resorting to the quantum regression theorem [42,43], we find the two-time correlations along the z spin direction to obey the following differential equations:

$$\frac{\partial}{\partial\tau}\langle S^z_j(t_1+\tau)S^z_{j+d}(t_1)\rangle = \sum_l G_{j,l}\langle S^z_l(t_1+\tau)S^z_{j+d}(t_1)\rangle,$$

where $\tau = t_2-t_1$, $G_{j,l} = \frac{D}{2}(\delta_{j+1,l}+\delta_{j-1,l}-2\delta_{j,l})$, $D = \frac{J_x^2}{\hbar^2\gamma}$, and the initial condition, $\langle S^z_j(t_1)S^z_{j+d}(t_1)\rangle$, is the solution of the equal-time correlations at t_1 [see Eq. (B1) of Appendix B]. While these equations are in principle valid only for $J_z=0$ and more complicated expressions are obtained for finite J_z, we find that for sufficiently large $\hbar\gamma/J_z$ their solution and in particular the extracted scaling coincide well with the t-MPS results. As illustrated in Fig. 2(b), for large $\hbar\gamma/J_z$, adiabatic elimination describes two-time correlations over the whole range of t_2/t_1, while for smaller ratios, this analytical approach describes well the long-time $(t_2/t_1)^{-3/2}$ scaling but fails to capture the initial dynamics. The overall good agreement between the t-MPS simulations and the adiabatic elimination approach within the scaling regime points to the diffusive nature of the propagation of the two-time correlations under

the action of dephasing. One should also note that this regime is also present if the initial state is not the Néel state but is instead made of larger domains with alternating magnetization.

Finally, the aging dynamics displayed by the correlations in the z spin direction should be contrasted with the evolution of the two-time correlations along the other spin directions. For the latter, the evolution leaves the dissipation-free subspace through the application of the lowering/rising operator $S^{\pm}_{l+d}$ at t_1. As a consequence, the dissipator strongly alters the evolution, and these correlations decay exponentially as a function of $t_2 - t_1$: $\langle S^+_i(t_2) S^-_j(t_1)\rangle \propto e^{-\beta(\gamma)(t_2-t_1)}$, where β is a function of the dissipative strength γ (see Ref. [12]).

Another interesting regime occurs solely at larger values of the interaction anisotropy J_z/J_x and for particular initial states. As shown in Fig. 1, for intermediate values of the time difference, $t_2 - t_1$, we find the two-time correlations along the z direction to follow a stretched exponential: $\log|C_d(t_2,t_1)| \sim (t_2-t_1)^{\nu_d}$, where ν_d depends on the system parameters. We checked that this regime persists at least for distances up to $d = 9$ in a system of size $L = 48$. This regime originates via the occurrence of nucleation events of energetically costly excitations. For the disordered XXZ model, using classical approximations, a similar regime displaying a stretched exponential decay was previously identified for the special case of $t_1 = 0$ where the two-time correlation reduces to the single-time staggered magnetization [13]. In comparison, here we identify this regime for actual two-time correlation functions over a wide range of t_1 using numerically exact simulations within the t-MPS formalism (see Fig. 1). Interestingly, even for large interaction anisotropy, this stretched exponential regime gives way to the scaling regime discussed above at larger t_2/t_1 ratios. These two contiguous regimes are displayed in Figs. 1 and 2 for the parameters $t_1 J_x = 5\hbar$, $\hbar\gamma = 10 J_x$ and $J_z = 2J_x$.

The mechanism behind the crossover between the stretched exponential and the algebraic regimes can be inferred by considering the proliferation of excitations caused by the dephasing noise. We expect the stretched exponential regime to be dominant only if well-separated timescales exist for the nucleation (or annihilation) of an excitation and for its motion. This separation typically occurs only for states on the lower and upper bounds of the spectrum of the XXZ model (see the well-separated energy bands at the boundaries of the spectrum in the inset of Fig. 3).

As the dissipative evolution brings the system into the infinite-temperature state, where all Hamiltonian levels are equally occupied, we expect the stretched exponential to show up only in the initial dynamics when the states at the boundaries of the spectrum are predominantly occupied. This situation explains the presence of the crossover from the stretched exponential to the algebraic regime seen in Figs. 1 and 2 (upper panels) for the parameters $t_1 J_x = 5\hbar$, $\hbar\gamma = 10 J_x$, and $J_z = 2J_x$, where the initial state is the classical Néel state which, for $J_z > 0$, lies near the lower edge of the energy spectrum. The time interval over which this regime occurs increases in width with the anisotropy strength, since for large interaction anisotropies, the difference between the intra and interband rates grows towards the edge of the spectrum. If the initial state is the Néel state, for $d = 1$ we observe that its region of existence terminates approximately when the two-time correlation becomes zero for the first time.

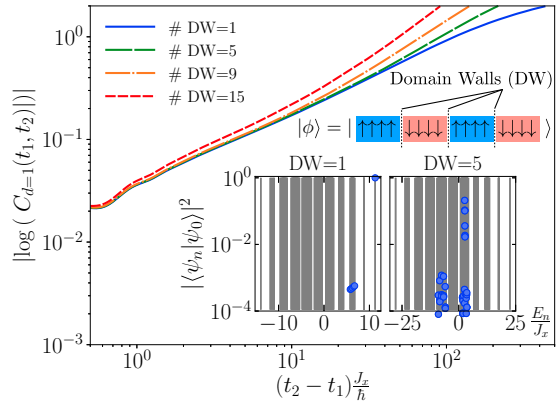

FIG. 3. Hierarchical dynamics. By increasing the number of domain walls (DW, see sketch in the figure) in the initial state, the dynamics of the two-time correlation function evolves faster from a regime where it follows a stretched exponential towards an algebraic region. The full quantum evolution obtained by t-MPS is shown for $L = 64, J_z = 10J_x, \hbar\gamma = 2J_x$, and $t_1 J_x = 5\hbar$. The inset shows the overlap (blue circles) of initial states with different numbers of domain walls with the energy eigenstates (gray vertical lines) of H_{XXZ} computed with exact diagonalization for a system of size $L = 12$ (with open boundary conditions) and $J_z = 10J_x$. The results have been computed using a Trotter time step of $\Delta t J_x/\hbar = 0.025$ and a truncation error of $\epsilon = 10^{-12}$.

To test this further, we consider different initial states with zero total magnetization and a well-defined number of domain walls. For the XXZ spin chain with $J_z > 0$, we first consider the state with one domain wall, which should have the largest energy among this subset of states. As illustrated in the inset of Fig. 3, for a system of $L = 12$ sites with a large interaction anisotropy one finds, using exact diagonalization, that the state with one domain wall has indeed strong overlap with only the most excited levels of the system and that these levels are all well separated from the others by energy gaps. The dephasing dynamics will then deexcite this state, but the rate of deexcitation to lower bands will be small compared to the rate to change this state within its own band. In contrast, considering the state with five domain walls, we find that it overlaps with levels located near the center of the Hamiltonian spectrum, where the energy bands are not well separated (see inset of Fig. 3). In fact, for larger system sizes, these bands will get closer and closer together. In this case, there is no pronounced separation of scale between the intra- and interband rate and the stretched exponential regime will be absent.

Comparing evolutions originating from states with increasing number of domain walls in Fig. 3, we find that the two-time correlations enter the stretched exponential regime only when the dissipative evolution begins from a state on the outer edge of the spectrum that is well separated in energy from the other states (thanks to strong interactions), confirming the picture detailed earlier. For initial states located within the center of the spectrum, where no clear separation of energy scales between the band gaps and bandwidths is present, the

evolution quickly enters the algebraic regime. Thus, using the initial state as a knob, one can tune the system dissipative dynamics and unveil features of the entire underlying Hamiltonian spectrum.

IV. CONCLUSION

Considering the evolution of two-time correlations, we highlighted the extremely rich and intricate physics at play in strongly interacting systems in contact with an environment. Using a numerically exact approach, we evaluated these correlations along all spin directions, extending dissipative MPS to two-time correlations. We showed that their evolution is nontrivially affected by the presence of a dissipative coupling, even leading to the breakdown of time-translation invariance. Perhaps most importantly, we demonstrated that the dissipative heating dynamics reveals fundamental spectral features of the underlying Hamiltonian. This finding paves the way to the development of nonequilibrium techniques to probe the spectrum of strongly correlated many-body systems.

ACKNOWLEDGMENTS

We thank I. Lesanovsky and M. Fleischhauer for enlighting discussions. We acknowledge support from the Singapore Ministry of Education (D.P.), the Singapore Academic Research Fund Tier-II (Projects No. MOE2016-T2-1-065 and No. WBS R-144-000-350-112) (D.P.), the DFG (Project No. 277625399-TRR 185 - project B4, and CRC 1238 Project No. 277146847 - project C05, and Einzelantrag), and the ERC (Grant No. 648166).

APPENDIX A: ADIABATIC ELIMINATION FORMALISM

At sufficiently large times, irrespective of the spin-spin interaction strength, the dissipation-free subspace will be reached. While this subspace is highly degenerate with respect to the dissipator, the Hamiltonian can possibly lift this degeneracy. In order to understand the nonequilibrium dynamics taking place, we perform adiabatic elimination, revealing how spin-flip–induced virtual excitations around the dissipation-free subspace affect the evolution of the system. For the system under study, in the presence of periodic boundary conditions, the dissipation-free subspace can be written down as $\rho_0 = \sum_{\vec{\sigma}} \rho_{0,\vec{\sigma}} |\vec{\sigma}\rangle\langle\vec{\sigma}|$, where the different spin configurations are labeled within the z-component basis such that $\vec{\sigma} = (\sigma_1, \sigma_2, \ldots, \sigma_L)$ with $\sigma_l = \pm 1/2$. For times larger than $1/\gamma$, the density matrix evolution is then effectively described by the set of differential equations

$$\frac{\partial \rho_{0,\vec{\sigma}}}{\partial t} = \sum_{j=1}^{L} \frac{J_x^2 \gamma}{2[(J_z \alpha_j)^2 + (\hbar\gamma)^2]} \delta_{\sigma_j, \bar{\sigma}_{j+1}} (\rho_{0,\vec{\sigma}_j} - \rho_{0,\vec{\sigma}}),$$

where $\alpha_j = 2(\sigma_{j-1}\sigma_j + \sigma_{j+1}\sigma_{j+2})$, $\vec{\sigma}_j$ is the spin configuration $\vec{\sigma}$ with swapped spins at site j, and $j+1$ and $\bar{\sigma}_j = -\sigma_j$.

APPENDIX B: EQUAL-TIME CORRELATIONS

Within adiabatic elimination, the equal-time correlations can be calculated in two different ways. Using kinetic Monte Carlo, we can solve numerically for ρ_0 and then compute the correlations, while in a second approach, valid for $\hbar\gamma \gg J_z$, we use the differential equation found above for ρ_0 to write down a set of coupled differential equations for $\hbar^2 C_{j,j+d}(t_1, t_1) = \langle S_j^z(t_1) S_{j+d}^z(t_1)\rangle$. Together with periodic boundary conditions, these equations take the form

$$\begin{aligned}
\frac{\partial}{\partial t_1} C_{j,j\pm1}(t_1,t_1) &= \frac{D}{2}(C_{j\mp1,j\pm1} + C_{j,j\pm2} - 2C_{j,j\pm1}),\\
\frac{\partial}{\partial t_1} C_{j,j+d}(t_1,t_1) &= \frac{D}{2}(C_{j+1,j+d} + C_{j-1,j+d} + C_{j,j+d+1}\\
&\quad + C_{j,j+d-1} - 4C_{j,j+d}), \quad \text{for } |d| > 1,
\end{aligned} \tag{B1}$$

where $D = \frac{J_x^2}{\hbar^2\gamma}$ and here $C_{l,l+d}$ stands for $C_{l,l+d}(t_1, t_1)$. If the system is initially prepared in the Néel state, the correlations are translationally invariant, $C_d(t_1, t_1) = C_{j,j+d}(t_1, t_1)$, with the equations

$$\begin{aligned}
\frac{\partial}{\partial t_1} C_{\pm1}(t_1,t_1) &= D(C_{\pm2} - C_{\pm1}),\\
\frac{\partial}{\partial t_1} C_d(t_1,t_1) &= D(C_{d+1} + C_{d-1} - 2C_d), \quad \text{for } |d| > 1,
\end{aligned}$$

and one should note that $C_d = C_{-d}$. To solve this system of differential equations, it is advantageous to redefine the equal-time correlations such that the evolution for all distances is described by a differential equation of the same form. To do so, we redefine the correlations as $\tilde{C}_d(t_1, t_1) = C_d(t_1, t_1)$ for $d \geqslant 1$ and $\tilde{C}_{d+1}(t_1, t_1) = C_d(t_1, t_1)$ for $d \leqslant -1$, implying that $\tilde{C}_d(t_1, t_1) = \tilde{C}_{-d+1}(t_1, t_1)$ for $d \geqslant 1$. One can then write down a diffusion equation for $\tilde{C}_d$ with diffusion constant D and periodic boundary condition

$$\frac{\partial}{\partial t_1} \tilde{C}_d(t_1,t_1) = D(\tilde{C}_{d+1} + \tilde{C}_{d-1} - 2\tilde{C}_d),$$

valid for $-\frac{L}{2} + 2 \leqslant d \leqslant \frac{L}{2}$. This equation can be solved analytically in terms of the modified Bessel functions $I_n(x)$ and has for the solution

$$\begin{aligned}
\tilde{C}_d(t_1,t_1) &= \frac{1}{4} e^{-2Dt_1}\\
&\quad \times \left(-I_d(2Dt_1) + \sum_{j=-\frac{L}{2}+2}^{\frac{L}{2}} (-1)^j \mathrm{sgn}(j) I_{d-j}(2Dt_1) \right).
\end{aligned}$$

For $d \geqslant 1$, in the limit where $L \gg 1$, the equal-time correlations take the form

$$C_d(t_1,t_1) = \frac{(-1)^d}{4} e^{-2Dt_1} \sum_{j=1-d}^{d-1} (-1)^j I_j(2Dt_1), \tag{B2}$$

and, furthermore, in the long-time limit, $Dt_1 \gg 1$, when $I_n(x) \sim e^x/\sqrt{2\pi x}$, these correlations simplify to

$$C_d(t_1,t_1) \sim -\frac{1}{\sqrt{64\pi Dt_1}}.$$

Therefore, equal-time correlations scale in time as $t_1^{-1/2}$, in agreement with t-MPS simulations as seen in Fig. 4(a). In fact, due to the form of the differential equations, one can infer that equal-time correlations propagate diffusively under

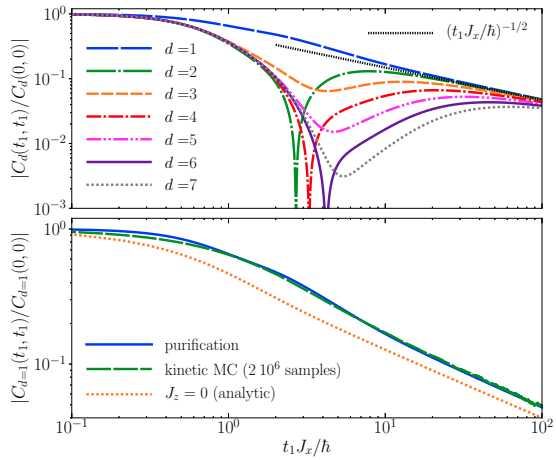

FIG. 4. Equal-time correlations. The upper panel shows the approach of a regime with diffusive dynamics for the normalized equal-time correlations, $|C_d(t_1,t_1)/C_d(0,0)|$, for spins separated by different distances d where $\hbar^2 C_d(t_1,t_1) = \langle S^z_{\frac{L}{2}}(t_1) S^z_{\frac{L}{2}+d}(t_1)\rangle$. The thin dotted black line is a guide to the eye highlighting the scaling at long times. The lower panel compares the full quantum evolution of the density matrix, with a kinetic Monte Carlo simulation of the evolution within the dissipation-free subspace, and with the solution obtained by solving the differential equations presented at Eq. (B1). Parameters are $\hbar\gamma = 2J_x$, $L = 80$, and $J_z = 2J_x$.

the action of the dephasing environment. In Fig. 4(b), one sees that all three methods, kinetic Monte Carlo, analytical adiabatic elimination, and t-MPS, predict the same scaling behavior at large times. While parallel, the analytical curve appears slightly below the two other ones; this discrepancy arises as obtaining an analytical solution requires one to set $J_z = 0$. However, even for finite J_z, the agreement between the analytical and the two other solutions gets better as the ratio $\hbar\gamma/J_z$ increases.

APPENDIX C: TWO-TIME CORRELATIONS

The long-time scaling of two-time correlations can also be understood analytically. In this case, to make progress, one needs to resort to adiabatic elimination and also make use of the quantum regression theorem [42,43]. As within adiabatic elimination, for times larger than $1/\gamma$ and for $\hbar\gamma \gg J_z$, the evolution of $\langle S^z_j(t)\rangle$ is governed by the linear differential equation

$$\frac{\partial}{\partial t_1}\langle S^z_j\rangle = \frac{D}{2}\sum_{l=1}^{L}(\delta_{j+1,l}+\delta_{j-1,l}-2\delta_{j,l})\langle S^z_l\rangle = \sum_{l=1}^{L} G_{j,l}\,\langle S^z_l\rangle, \tag{C1}$$

and the quantum regression theorem states that the two-time correlation functions

$$\hbar^2 C_{j,j+d}(t_1+\tau,t_1) = \langle S^z_j(t_1+\tau) S^z_{j+d}(t_1)\rangle$$

should be described by the differential equations

$$\frac{\partial}{\partial\tau} C_{j,j+d}(t_1+\tau,t_1) = \sum_{l=1}^{L} G_{j,l}\, C_{l,j+d}(t_1+\tau,t_1),$$

where $G_{j,l}$ are the same matrix elements as in Eq. (C1). Assuming once again spatial translation invariance, this set of equations reduces to a smaller set of diffusive equations for $C_d(t_1+\tau,t_1)$ with diffusion constant $\frac{D}{2}$,

$$\frac{\partial}{\partial\tau} C_d(t_1+\tau,t_1) = \frac{D}{2}(C_{d+1}+C_{d-1}-2C_d),$$

where C_l stands for $C_l(t_1+\tau,t_1)$. Solving this set of differential equations, we find the two-time correlations along the z direction to evolve as

$$C_d(t_2,t_1) = e^{-D(t_2-t_1)} \sum_{d'=-\frac{L}{2}+1}^{\frac{L}{2}} C_{d'}(t_1,t_1)\, I_{d-d'}(D(t_2-t_1)),$$

where $t_2 = t_1+\tau$. Then, using as initial conditions $C_d(t_1,t_1)$ obtained in Eq. (B2) for $d \geqslant 1$ together with $C_{d=0}(t_1,t_1) = \frac{1}{4}$ and $C_{-d}(t_1,t_1) = C_d(t_1,t_1)$, we find for $d \geqslant 0$, in the limit $L \gg 1$, that the two-time correlations can be rewritten in the more amenable form

$$\begin{aligned} C_d(t_2,t_1) = {} & \frac{1}{4} e^{-D(t_2-t_1)} I_d(D(t_2-t_1)) \\ & - \frac{1}{4}\,\delta_{0,d}\, e^{-D(t_2+t_1)} I_0(D(t_2+t_1)) \\ & + \frac{(-1)^d}{4}(1-\delta_{0,d})\, e^{-D(t_2+t_1)} \\ & \times \sum_{j=1-d}^{d-1} (-1)^j I_j(D(t_2+t_1)) + G_d(t_2,t_1), \end{aligned} \tag{C2}$$

where

$$\begin{aligned} G_d(t_2,t_1) = {} & e^{-D(t_2-t_1)} \sum_{d'=1}^{\infty} C_{d'}(t_1,t_1) \\ & \times (I_{d+d'}(D(t_2-t_1)) - I_{d+d'-1}(D(t_2-t_1))). \end{aligned} \tag{C3}$$

Using this expression, we then evaluate the scaling of the normalized two-time correlations in the limit $Dt_2 \gg Dt_1 \gg 1$. While for the first three terms of Eq. (C2), we simply expand $I_n(x)$ for large x, for $G_d(t_1,t_2)$, we also need to take the continuum limit in order to carry out analytically the sum over d'. This additional limit amounts to approximate $C_{d'}(t_1,t_1)$ in Eq. (C3) as

$$C_{d'}(t_1,t_1) \sim -\frac{1}{4}\frac{1}{\sqrt{2\pi(2Dt_1)}}\, e^{-\frac{1}{2}\frac{d'^2}{2Dt_1}}.$$

For $|d| \geqslant 1$, the normalized two-time correlations therefore scale as

$$\begin{aligned} \frac{C_d(t_2,t_1)}{C_d(t_1,t_1)} \sim {} & -\sqrt{2}\left(\frac{t_2}{t_1}\right)^{-\frac{3}{2}} \\ & \times \left(1+\frac{1}{\sqrt{\pi}}(Dt_1)^{-\frac{1}{2}} - \frac{1}{4}(Dt_1)^{-1}\right). \end{aligned}$$

Thus, for very large Dt_1, only the leading contribution remains and the normalized two-time correlations scale as

$$\left|\frac{C_d(t_2,t_1)}{C_d(t_1,t_1)}\right| \sim \sqrt{2}\left(\frac{t_2}{t_1}\right)^{-\frac{3}{2}}, \quad |d| \geqslant 1,$$

which is in agreement with the results obtained from t-MPS. This result highlights that aging dynamics can emerge from diffusive processes triggered by dephasing noise. Finally, for $d = 0$, where $C_0(t_1, t_1) = \frac{1}{4}$, the long-time limit of the normalized two-time correlation scales as

$$\frac{C_0(t_2,t_1)}{C_0(t_1,t_1)} \sim \frac{1}{\sqrt{2\pi}} (Dt_1)^{-\frac{1}{2}} \left(\frac{t_2}{t_1}\right)^{-\frac{3}{2}} \times \left(1 + \frac{1}{\sqrt{\pi}}(Dt_1)^{-\frac{1}{2}} - \frac{1}{4}(Dt_1)^{-1}\right).$$

Consequently, on-site two-time correlations break time-translational invariance and scale algebraically; however, to leading order, these correlations do not solely depend on the ratio t_2/t_1 and thus do not display aging.

APPENDIX D: EVOLUTION OF THE PURIFIED DENSITY MATRIX WITHIN THE TIME-DEPENDENT MATRIX PRODUCT STATE (t-MPS) METHOD

In this section we demonstrate that the representation of quantum states in terms of matrix product states (MPS) [35] offers a well-controlled way to efficiently encode the quantum many-body density matrix of interacting open quantum systems and to simulate dissipative Lindblad dynamics numerically [9,40]. By introducing a second copy of the original Hilbert space $\mathcal{H}$, the density matrix can be rewritten as a pure state in the superspace $\mathcal{H} \otimes \mathcal{H}$. This concept is known from the representation of mixed states appearing in finite temperature simulations [35,38,44], but there are a few important differences. Here we purify the basis $|\vec{\sigma}\rangle \langle \vec{\sigma}'|$ of the density matrix using the prescription

$$|\sigma_1, \sigma_2, \ldots \sigma_L\rangle \langle \sigma_1', \sigma_2', \ldots \sigma_L'| \longrightarrow |\sigma_1\sigma_1'\sigma_2\sigma_2' \ldots \sigma_L\sigma_L'\rangle\!\rangle,$$

where $|\ldots\rangle\!\rangle$ denotes a purified state including two different spin species $\{\sigma_l, \sigma_l'\}$. The first species labeled by σ and the second species labeled by σ' are arranged alternately in position. Thus the density matrix in the new basis is written as

$$\rho = \sum_{\vec{\sigma},\vec{\sigma}'} \rho_{\vec{\sigma},\vec{\sigma}'} |\vec{\sigma}\rangle \langle \vec{\sigma}'| \longrightarrow$$

$$|\rho\rangle\!\rangle = \sum_{\vec{\sigma},\vec{\sigma}'} \rho_{\vec{\sigma},\vec{\sigma}'} |\sigma_1\sigma_1'\sigma_2\sigma_2' \ldots \sigma_L\sigma_L'\rangle\!\rangle.$$

The coefficients of the purified density matrix state can be written in the MPS form as

$$\rho_{\vec{\sigma},\vec{\sigma}'} = M^{\sigma_1} M^{\sigma_1'} M^{\sigma_2} M^{\sigma_2'} \ldots M^{\sigma_L} M^{\sigma_L'}.$$

We consider product states as initial states in this work; thus the corresponding MPS representation of the purified initial density matrix is exact with bond dimension equal to 1. Nevertheless, this purification step can also be generalized to states with finite bond dimension accompanied with a subsequent compression scheme [45],

$$\mathbb{L} = -\frac{i}{\hbar}\left(H_{\mathrm{XXZ}} \otimes I + I \otimes H_{\mathrm{XXZ}}^T\right) + \gamma \sum_{l=1}^{L} \left(S_l^z \otimes S_l^z - \frac{1}{4} I \otimes I\right), \tag{D1}$$

where I is the identity operator acting on Hilbert space $\mathcal{H}$ and H_{XXZ}^T is the transpose of the Hamiltonian. We understand the tensor product in a way such that the first component is acting on the spins $\vec{\sigma}$ and the second on the spins $\vec{\sigma}'$. In the model under study, the original Hamiltonian acts on the nearest-neighbor sites and the jump operators are localized to a single site. Consequently, spins σ_l and σ_{l+1} as well as spins σ_l' and σ_{l+1}' are coupled via a next-nearest-neighbor interaction due to the Hermitian part of the evolution [the first and second terms in Eq. (D1)] while spins σ_l and σ_l' are coupled via a nearest-neighbor interaction through the dissipative part $S_l^z \otimes S_l^z$ [the third term in Eq. (D1)]. We extend the concept of t-MPS techniques for Hamiltonian dynamics with next-nearest-neighbor interactions to the dissipative evolution of purified density matrices by splitting the Lindbladian into a sum of terms each covering in total four sites. We regroup these four-site contributions for the Trotter evolution as

$$\mathbb{L} = \sum_{l=1}^{\frac{L}{2}} \mathbb{L}_{2l-1} + \sum_{l=1}^{\frac{L}{2}-1} \mathbb{L}_{2l} \equiv \mathbb{L}_{\mathrm{odd}} + \mathbb{L}_{\mathrm{even}}, \tag{D2}$$

with

$$\begin{aligned}\mathbb{L}_l = -\frac{i}{\hbar}\Bigg[& \frac{J_x}{2}\left(S_l^+ S_{l+1}^- \otimes I + S_l^- S_{l+1}^+ \otimes I \right. \\ & \left. - I \otimes S_l^+ S_{l+1}^- - I \otimes S_l^- S_{l+1}^+\right) \\ & + J_z \left(S_l^z S_{l+1}^z \otimes I - I \otimes S_l^z S_{l+1}^z\right) \\ & + \gamma \left\{\left(S_l^z \otimes S_l^z - \frac{1}{4} I \otimes I\right)\right. \\ & \left. + \delta_{l,L-1}\left(S_L^z \otimes S_L^z - \frac{1}{4} I \otimes I\right)\right\}\Bigg].\end{aligned}$$

In analogy to Eq. (D1), the tensor products combining four operators should be interpreted such that the first part of the tensor product acts on the spins $\vec{\sigma}$ and the second part on the spins $\vec{\sigma}'$. We approximate the time evolution operator by the second-order Suzuki-Trotter decomposition [46]

$$\mathrm{e}^{\mathbb{L}\Delta t} = \mathrm{e}^{\mathbb{L}_{\mathrm{odd}}\Delta t/2} \mathrm{e}^{\mathbb{L}_{\mathrm{even}}\Delta t} \mathrm{e}^{\mathbb{L}_{\mathrm{odd}}\Delta t/2} + \mathcal{O}(L\Delta t^3).$$

The Lindblad evolution can then be computed similarly to the standard t-MPS algorithm by a sequence of gate applications followed by a compression according to a truncation scheme. Taking the two possible spin directions of each site into account, the contraction of the four-site time evolution gates with the MPS increases the dimension of the two outer bonds of the selected four sites from m to 2^2m. The dimension of the central bonds increases from m to 2^4m and a subsequent compression is needed.

For unitary systems, strategies have been developed to take good quantum numbers into account in order to improve the performance of t-MPS algorithms and slow down the growth of the MPS bond dimension [35]. Here, we extend this approach to dissipative systems by exploiting the conservation of the equivalent of the total magnetization in the purified superspace $M_{\mathrm{tot}} = \sum_{l=1}^{L} (S_l^z \otimes I + I \otimes S_l^z)$ by the Lindblad evolution within one single symmetry block. This enables us to investigate the long-time behavior of the considered two-time correlation functions. The encoding of the conservation

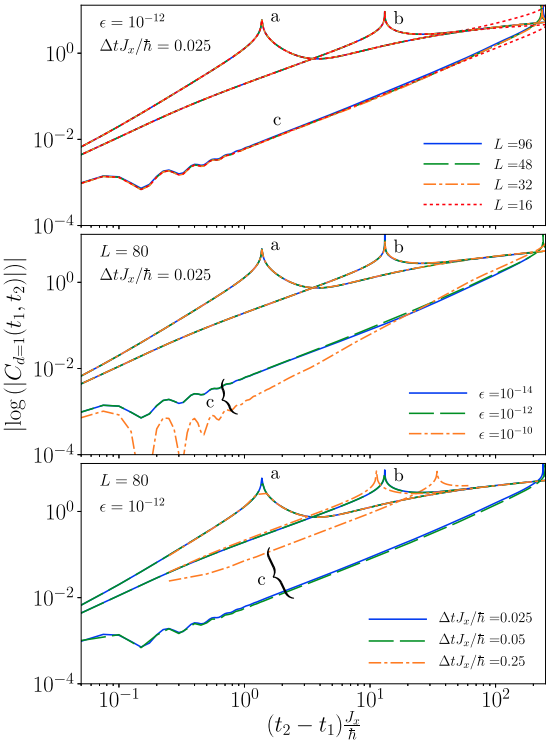

FIG. 5. Convergence analysis for the stretched exponential regime. We present data for the logarithm of the two-time correlations as a function of the difference between the two application times for three parameter sets labeled a, b, and c, where $(t_{1,\mathrm{a}}J_x/\hbar,\ \hbar\gamma_\mathrm{a}/J_x,\ J_{z,\mathrm{a}}/J_x) = (5, 2, 1)$, $(t_{1,\mathrm{b}}J_x/\hbar,\ \hbar\gamma_\mathrm{b}/J_x,\ J_{z,\mathrm{b}}/J_x) = (5, 10, 2)$, and $(t_{1,\mathrm{c}}J_x/\hbar, \hbar\gamma_\mathrm{c}/J_x, J_{z,\mathrm{c}}/J_x) = (5, 2, 40)$. (Upper panel) Comparing results for different system sizes L and time step $\Delta t = 0.025\hbar/J_x$ and truncation weight $\epsilon = 10^{-12}$, shows that, up to the considered time t_2, the boundary effects are absent for $L \geqslant 32$. (Middle panel) Varying the truncation weight for the different parameter sets for system size $L = 80$ and time step $\Delta t = 0.025\hbar/J_x$, the data collapses to the same curve for $\epsilon \leqslant 10^{-12}$. (Lower panel) Different time steps for system size $L = 80$ and truncation error $\epsilon = 10^{-12}$ demonstrates that a time step of $\Delta t J_x/\hbar = 0.05$ is sufficiently small to simulate the full quantum evolution in the time interval considered.

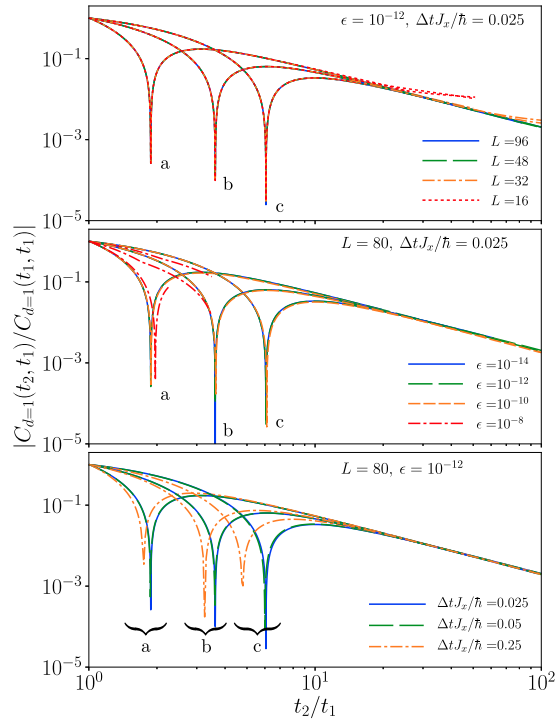

FIG. 6. Convergence analysis for the scaling regime. We investigate the t-MPS convergence for the normalized two-time correlation function as a function of the ratio of the two application times (t_2/t_1) for three different parameter sets labeled by a, b, and c with $(t_{1,\mathrm{a}}J_x/\hbar,\ \hbar\gamma_\mathrm{a}/J_x,\ J_{z,\mathrm{a}}/J_x) = (10, 10, 2)$, $(t_{1,\mathrm{b}}J_x/\hbar,\ \hbar\gamma_\mathrm{b}/J_x,\ J_{z,\mathrm{b}}/J_x) = (5, 10, 2)$, and $(t_{1,\mathrm{c}}J_x/\hbar,\ \hbar\gamma_\mathrm{c}/J_x,\ J_{z,\mathrm{c}}/J_x) = (5, 16, 2)$. We conduct a convergence analysis analogous to the one shown on Fig. 5. We consider the system size in the upper panel, the truncation error in the middle panel, and the time step in the lower panel. From this analysis, we conclude that the simulation results are converged for $L \geqslant 48$, $\epsilon \leqslant 10^{-10}$, and a time step of $\Delta t J_x/\hbar = 0.05$.

laws in the dissipative MPS algorithm is more involved than in its unitary counterpart. In particular, the calculation of expectation values needs to be performed in a clever way using a transformation as described in the following in order to remain numerically manageable. In the framework of purification, the trace representation of expectation values translates to the following scalar product [47]:

$$\langle A\rangle = \frac{\mathrm{tr}(A\rho)}{\mathrm{tr}(\rho)} = \frac{\langle\langle \mathbb{1}|A|\rho\rangle\rangle}{\langle\langle \mathbb{1}|\rho\rangle\rangle}, \text{ with } |\mathbb{1}\rangle\rangle = \bigotimes_{l=1}^{L}\sum_{\sigma_l=\pm 1/2}|\sigma_l\sigma_l\rangle\rangle.$$

Restricting the state $|\mathbb{1}\rangle\rangle$ to a single quantum number sector can result in strongly entangled many-body states, which are not efficiently representable in MPS form. To solve this problem we introduce a unitary transformation acting on each of the second spin species such that the total magnetization is distributed equally over all individual pairs of two spin species which contribute to $|\mathbb{1}\rangle\rangle$. For the symmetry sector with zero magnetization ($M_\mathrm{tot} = 0$), one possible transformation is given by $\mathbb{U} = \bigotimes_{l=1}^{L}(I_l \otimes 2/\hbar S_l^x)$, which transforms the state $|\mathbb{1}\rangle\rangle$ to

$$\mathbb{U}|\mathbb{1}\rangle\rangle = \bigotimes_{l=1}^{L}[|\uparrow\downarrow\rangle\rangle + |\downarrow\uparrow\rangle\rangle].$$

This decomposition of $|\mathbb{1}\rangle\rangle$ into spin triplets offers a very efficient MPS representation with an alternating bond dimension of 2 and 1. Finally, with this transformation all operators including the Lindbladian superoperator and the density matrix need to be transformed accordingly,

$$\mathbb{L} \longrightarrow \mathbb{U}^\dagger\mathbb{L}\mathbb{U}$$
$$|\rho(t=0)\rangle\rangle \longrightarrow \mathbb{U}|\rho(t=0)\rangle\rangle.$$

To evolve the system in time, we apply the four-sites gates on the transformed initial density matrix, and observables are subsequently measured.

In the following we discuss the accuracy of results obtained from the t-MPS algorithm. To this end we present convergence analyses for the stretched exponential region as summarized in Fig. 5 as well as for the scaling regime in Fig. 6. As we are aiming to understand the behavior of the system in the thermodynamic limit, we need to guarantee the

absence of boundary effects by verifying the consistency for different system sizes L (see upper panel in Figs. 5 and 6). Furthermore, the compression of the MPS by truncating the low end of the singular value spectrum of the density matrix plays an important role. This approximation is controlled by the sum of truncated singular values known as the truncation weight ϵ, which is fixed to a very small value, resulting in an estimate of the MPS with an accuracy close to machine precision (see middle panel in Figs. 5 and 6). Finally, the convergence with regard to the time step $\Delta t J_x/\hbar$ needs to be monitored in order to confirm the validity of the Suzuki-Trotter decomposition (see lower panel in Figs. 5 and 6). Observing the results in Fig. 5, we conclude that considering the system of size $L = 32$, a truncation weight of $\epsilon = 10^{-12}$ and a time step of $\Delta t J_x/\hbar = 0.05$ is sufficient to confirm the stretched exponential regime. The convergence curves shown in Fig. 6 show that a system size of $L = 48$, a truncation weight of $\epsilon = 10^{-10}$, and a time step of $\Delta t J_x/\hbar = 0.05$ is sufficient to compute the considered two-time correlations in the time interval relevant for the scaling dynamics.

[1] N. W. Ashcroft and N. D. Mermin, *Solid State Physics* (Thomson Learning, Boston, 1976).

[2] T. Stöferle, H. Moritz, C. Schori, M. Köhl, and T. Esslinger, Phys. Rev. Lett. **92**, 130403 (2004).

[3] J. T. Stewart, J. P. Gaebler, and D. S. Jin, Nature (London) **454**, 744 (2008).

[4] T. Esslinger, Annu. Rev. Condens. Matter Phys. **1**, 129 (2010).

[5] D. Lu, I. M. Vishik, M. Yi, Y. Chen, R. G. Moore, and Z.-X. Shen, Annu. Rev. Condens. Matter Phys. **3**, 129 (2012).

[6] S. T. Bramwell and B. Keimer, Nat. Mater. **13**, 763 (2014).

[7] E. Vincent and V. Dupuis, in *Frustrated Materials and Ferroic Glasses* edited by T. Lookman and X. Ren, Springer Series in Materials Science (Springer, Cham, 2018), Vol. 275, pp. 31–56.

[8] J. Marino and A. Silva, Phys. Rev. B **86**, 060408(R) (2012).

[9] J.-S. Bernier, R. Tan, L. Bonnes, C. Guo, D. Poletti, and C. Kollath, Phys. Rev. Lett. **120**, 020401 (2018).

[10] M. Buchhold and S. Diehl, Phys. Rev. A **92**, 013603 (2015).

[11] M. Marcuzzi, E. Levi, W. Li, J. P. Garrahan, B. Olmos, and I. Lesanovsky, New J. Phys. **17**, 072003 (2015).

[12] B. Sciolla, D. Poletti, and C. Kollath, Phys. Rev. Lett. **114**, 170401 (2015).

[13] B. Everest, I. Lesanovsky, J. P. Garrahan, and E. Levi, Phys. Rev. B **95**, 024310 (2017).

[14] L. He, L. M. Sieberer, and S. Diehl, Phys. Rev. Lett. **118**, 085301 (2017).

[15] Z. Denis and S. Wimberger, Condens. Matter **3**, 2 (2018).

[16] J. C. Halimeh, M. Punk, and F. Piazza, Phys. Rev. B **98**, 045111 (2018).

[17] D. Kilda and J. Keeling, Phys. Rev. Lett. **122**, 043602 (2019).

[18] R. R. W. Wang, B. Xing, G. G. Carlo, and D. Poletti, Phys. Rev. E **97**, 020202(R) (2018).

[19] T. Giamarchi, *Quantum Physics in One Dimension* (Oxford University Press, Oxford, 2004).

[20] G.-B. Jo, Y.-R. Lee, J.-H. Choi, C. A. Christensen, T. H. Kim, J. H. Thywissen, D. E. Pritchard, and W. Ketterle, Science **325**, 1521 (2009).

[21] K.-K. Ni, S. Ospelkaus, M. H. G. de Miranda, A. Pe'er, B. Neyenhuis, J. J. Zirbel, S. Kotochigova, P. S. Julienne, D. S. Jin, and J. Ye, Science **322**, 231 (2008).

[22] A. Friedenauer, H. Schmitz, J. T. Glueckert, D. Porras, and T. Schaetz, Nat. Phys. **4**, 757 (2008).

[23] K. Kim, M.-S. Chang, S. Korenblit, R. Islam, E. E. Edwards, J. K. Freericks, G.-D. Lin, L.-M. Duan, and C. Monroe, Nature (London) **465**, 590 (2010).

[24] J. Simon, W. S. Bakr, R. Ma, M. E. Tai, P. M. Preiss, and M. Greiner, Nature (London) **472**, 307 (2011).

[25] S. Murmann, F. Deuretzbacher, G. Zürn, J. Bjerlin, S. M. Reimann, L. Santos, T. Lompe, and S. Jochim, Phys. Rev. Lett. **115**, 215301 (2015).

[26] M. Saffman, T. G. Walker, and K. Mølmer, Rev. Mod. Phys. **82**, 2313 (2010).

[27] C. Gross and I. Bloch, Science **357**, 995 (2017).

[28] Y. S. Patil, S. Chakram, and M. Vengalattore, Phys. Rev. Lett. **115**, 140402 (2015).

[29] H. P. Lüschen, P. Bordia, S. S. Hodgman, M. Schreiber, S. Sarkar, A. J. Daley, M. H. Fischer, E. Altman, I. Bloch, and U. Schneider, Phys. Rev. X **7**, 011034 (2017).

[30] F. Letscher, O. Thomas, T. Niederprüm, M. Fleischhauer, and H. Ott, Phys. Rev. X **7**, 021020 (2017).

[31] Z. Cai and T. Barthel, Phys. Rev. Lett. **111**, 150403 (2013).

[32] D. Poletti, J.-S. Bernier, A. Georges, and C. Kollath, Phys. Rev. Lett. **109**, 045302 (2012).

[33] D. Poletti, P. Barmettler, A. Georges, and C. Kollath, Phys. Rev. Lett. **111**, 195301 (2013).

[34] S. R. White, Phys. Rev. Lett. **69**, 2863 (1992).

[35] U. Schollwöck, Ann. Phys. **326**, 96 (2011), January 2011 Special Issue.

[36] H. J. Mikeska and A. Kolezhuk, in *Quantum Magnetism*, edited by U. Schollwöck, J. Richter, D. Farnell, and R. Bishop, Lecture Notes in Physics Vol. 645 (Springer, New York, 2004), p. 1.

[37] ITensor C++ library, available at http://itensor.org.

[38] M. Zwolak and G. Vidal, Phys. Rev. Lett. **93**, 207205 (2004).

[39] F. Verstraete, M. M. Wolf, and J. I. Cirac, Nat. Phys. **5**, 633 (2009).

[40] L. Bonnes and A. M. Läuchli, arXiv:1411.4831.

[41] J. J. Garcia-Ripoll, S. Dürr, N. Syassen, D. M. Bauer, M. Lettner, G. Rempe, and J. I. Cirac, New J. Phys. **11**, 013053 (2009).

[42] C. Gardiner and P. Zoller, *Quantum Noise* (Spinger-Verlag, Berlin, 2000).

[43] H. P. Breuer and F. Petruccione, *The Theory of Open Quantum Systems* (Oxford University Press, Oxford, 2002).

[44] F. Verstraete, J. J. García-Ripoll, and J. I. Cirac, Phys. Rev. Lett. **93**, 207204 (2004).

[45] S. Wolff, Ph.D. Thesis, ULB University Bonn, 2019.

[46] N. Hatano and M. Suzuki, *Finding Exponential Product Formulas of Higher Orders* (Springer, Berlin/Heidelberg, 2005).

[47] J. Cui, J. I. Cirac, and M. C. Bañuls, Phys. Rev. Lett. **114**, 220601 (2015).